Geophysical Research Letters

RESEARCH LETTER
10.1029/2021GL097329

Key Points:

- Empirical models of Poynting flux are separately constructed for the northern and southern hemispheres using satellite data
- During local summer under active conditions, the northern hemisphere supports about 30% more total Poynting flux
- The most likely cause is the asymmetry in the geomagnetic field, which provides about 30% more conductance in the northern hemisphere

Supporting Information:

Supporting Information may be found in the online version of this article.

Correspondence to:

R. B. Cosgrove,
russell.cosgrove@me.com

Citation:

Cosgrove, R. B., Bahcivan, H., Chen, S., Sanchez, E., & Knipp, D. (2022). Violation of hemispheric symmetry in integrated Poynting flux via an empirical model. *Geophysical Research Letters*, *49*, e2021GL097329. https://doi.org/10.1029/2021GL097329

Received 7 DEC 2021
Accepted 27 JAN 2022

Author Contributions:

Conceptualization: Russell B. Cosgrove, Ennio Sanchez, Delores Knipp
Formal analysis: Russell B. Cosgrove
Funding acquisition: Russell B. Cosgrove, Hasan Bahcivan, Delores Knipp
Investigation: Russell B. Cosgrove, Hasan Bahcivan, Delores Knipp
Methodology: Russell B. Cosgrove, Hasan Bahcivan
Project Administration: Russell B. Cosgrove, Delores Knipp

Violation of Hemispheric Symmetry in Integrated Poynting Flux via an Empirical Model

Russell B. Cosgrove[1,2], Hasan Bahcivan[2], Steven Chen[3], Ennio Sanchez[2], and Delores Knipp[4,5]

[1]Florida Space Institute, University of Central Florida, Orlando, FL, USA, [2]Center for Geospace Studies, SRI International, Menlo Park, CA, USA, [3]LeoLabs, Inc., Menlo Park, CA, USA, [4]Smead Aerospace Engineering Science Department, University of Colorado Boulder, Boulder, CO, USA, [5]High Altitude Observatory, National Center for Atmospheric Research, Boulder, CO, USA

Abstract For southward interplanetary magnetic field (IMF) during local summer, the hemispherically integrated Poynting flux estimated by FAST-satellite-derived empirical models is significantly larger for the northern hemisphere (NH) than for the southern hemisphere (SH). In order to test whether the difference is statistically significant, the model uncertainties have been estimated by dividing the data sets for each hemisphere into two nonintersecting sets, and separately constructing the model using each of the four sets. The model uncertainty appears to be smaller than the estimated asymmetry. The asymmetry is mostly absent when the IMF is northward, except there is some evidence that it may actually reverse during local winter. The phenomena is coupled with what appears to be a more distinct two-cell convection pattern in the NH, and a possibly greater cusp contribution in the SH. All this suggests an effect of magnetosphere-ionosphere-thermosphere coupling, probably related to asymmetries in Earth's geomagnetic field.

Plain Language Summary Energy enters Earth's atmosphere in various forms, including sunlight, fast-moving particles, and also relatively low-frequency electric and magnetic fields. The later component is referred to as Poynting flux (PF), and is important to study because it produces density anomalies that can perturb satellite orbits in unexpected ways. PF is produced by a complex interaction of Earth's geomagnetic field and particle-populations with the solar wind coming from the sun, and is thus quite difficult to model through first principles physics. Data-based models of PF, known as empirical models, can be used to produce a sort of ground-truth for development and testing of the physics-based models, which demonstrate our understanding of the phenomenon, and which will eventually be needed to develop a predictive capability. A particularly useful feature in this regard is the symmetry, or lack thereof, between Earth's northern and southern hemispheres. The difference between the hemispheres is relatively subtle, and so successfully modeling the difference using first-principles physics would be a significant demonstration of understanding. In this work we provide an empirical assessment of the hemispheric symmetry of PF that can be used to provide such a discriminator.

1. Introduction

Empirical models of the incident Poynting flux (PF), associated with auroral processes, have been separately constructed for the northern and southern hemispheres using data from the Fast Auroral SnapshoT (FAST) satellite (Carlson et al. (1998)). The models are constructed by fitting a set of basis functions to the PF measured by the electric and magnetic field sensors on board FAST (Ergun et al. (2001); Elphic et al. (2001)), where the basis function coefficients are expressed as quadratic equations in a chosen set of geophysical parameters. The modeling methodology was explained in detail by Cosgrove et al. (2014), and has changed very little. Basis functions are constructed from the data as empirical orthogonal functions, and are used to describe variations from a background state that is essentially an IMF-average. However, the lead author has recently put the data itself through a process of quality control that has reduced the number of orbits deemed useable from 8,085 to 7,301 for the NH, and from 5,501 to 4,953 for the SH, with the benefit of providing additional confidence in the results presented here (which were noted earlier, but not published). Some details concerning the quality control process are given in the Supporting Information S1.

The models output flux maps for the regions above 60° magnetic latitude (MLAT) and below − 60° MLAT as a function of (a) clock angle of the interplanetary magnetic field (IMF), (b) magnitude of the IMF in the GSM y-z

Software: Russell B. Cosgrove
Supervision: Russell B. Cosgrove, Hasan Bahcivan
Validation: Russell B. Cosgrove, Hasan Bahcivan
Writing – original draft: Russell B. Cosgrove
Writing – review & editing: Russell B. Cosgrove, Hasan Bahcivan, Delores Knipp

plane ($B_\perp$), (c) solar wind speed (V_{sw}), (d) solar wind number density (N_{sw}), (e) magnetic dipole tilt angle (Dip angle), (f) the IMF GSM B_x component, and (g) the altitude above Earth (all PF densities are referenced (projected) to 100 km in altitude, for comparability). Minor changes that were made to the model include addition of the B_x and altitude parameters, and elimination of the AL-index parameter. Besides these the only change to the modeling methodology is that the basis functions and background states (shown in top two panels of Figure 3) are now constructed separately for the NH and SH.

Following is an analysis of the hemispherically integrated PF, based on the empirical models, and finding that the NH supports significantly more PF during active conditions (~30% more), under the mirror symmetries in Dip angle and B_y. The effects of IMF and Dip angle are presented, with V_{sw}, $B_\perp$, N_{sw}, and B_x held constant ($V_{sw} = 450$ km/s, $B_\perp = 5$ nT, $N_{sw} = 4$ cm^{-3}, $B_x = 0$ nT), since the latter four parameters do not seem to affect the symmetry (i.e., when $B_x = 0$ (Stubbs et al. (2005))).

To our knowledge this is the first article to find an overall asymmetry in the hemispherically integrated PF. However, there have recently appeared two articles that find asymmetries in regional PF related by magnetic conjugacy (Pakhotin et al. (2021); Knipp et al. (2021)). The most comparable of these is the analysis by Knipp et al. (2021), which considers what is sometimes called "quasi-static PF," that is, inclusive of all frequencies down to zero. This quantity represents the total incident PF. Knipp et al. (2021) use measurements from the Defense Meteorological Satellite Program (DMSP) to statistically compare localized conjugate regions (with >50% coverage) in the northern and southern hemispheres, and find that the NH tends to have more PF.

In the present study based on FAST data, we extend this result to a statement about the total hemispherically integrated PF, and also add some statistical rigor. By fitting the data to a parameterized model we are able to compare the two hemispheres under equivalent IMF and seasonal conditions, whereas the other studies must rely on the sheer size of the data sets to limit the effects of the sampling bias associated with the satellite passing through the hemispheres under different conditions. This approach also allows for the finding that the asymmetry is mostly associated with southward IMF, and is stronger during local summer. To make the conclusions more rigorous, we consider independent subdivisions of the FAST data and use them to make an estimate of the likelihood that the determination of asymmetry may be false. We find only a 10% chance of false alarm.

The second article (Pakhotin et al. (2021)) analyzes what is know as Alfvenic Poynting flux using data from the SWARM satellites. Alfvenic Poynting flux refers to the Poynting flux in a certain category of observed events with wave-like signatures (e.g., Janhunen et al. (2005); Hartinger et al. (2015); Luhr et al. (2015); Hatch et al. (2017); Keiling et al. (2019); Keiling (2021)), which are sometimes referred as Alfven or Alfvenic waves, where the later terminology is meant to capture the distinction from the low-frequency Alfven waves that are involved in setting up the steady-state ionospheric conductance (e.g., Lysak and Dum (1983); Cosgrove (2016); Pakhotin et al. (2018); Pakhotin et al. (2020); Keiling (2021)). Pakhotin et al. (2021) identify Alfvenic events in SWARM data and process the Poynting flux in three different ranges of spatial scale, as part of an argument that there is significant energy in the Alfvenic component (compare with Hartinger et al. (2015)). Then, making a statistical comparison of localized conjugate regions, Pakhotin et al. (2021) find that there is more Alfvenic Poynting flux in the NH.

In the present article we analyze the total Poynting flux, which includes the Alfvenic part as a component. The main reason to divide the Poynting flux into different frequency ranges is to sort it according to source regions and source types (e.g., Wing et al. (2010); Luhr et al. (2015)), which is beyond the scope of the Cosgrove et al. (2014) empirical model. It would seem that the total electromagnetic energy contribution is an appropriate subject for analysis, in addition to studies of the separate contributions.

There are also a few other kinds of north-south comparisons that are less directly related to the current study. Various authors have found an overall north-south asymmetry in the cross polar cap potential (Pettigrew et al. (2010); Förster and Haaland (2015)), or in the field aligned current (FAC) (Coxon et al. (2016); Workayehu et al. (2019); Shi et al. (2020)), or in the ion or convection velocities (Förster et al. (2007); Förster and Haaland (2015); Cnossen and Förster (2016)). Förster and Haaland (2015) also find an asymmetry in the appearance of the flow patterns. Also, some authors compare the summer and winter hemispheres (e.g., Papitashvili and Rich (2002)), or dark versus illuminated regions (Liou and Mitchell (2020)), or instantaneous conditions (Hong et al. (2021), a model-based study). Although less directly relevant, these kinds of studies provide complimentary information that may be useful in sorting out the causes of asymmetry.

We conclude the article with a simple argument invoking the well-documented asymmetry in the geomagnetic field, as the source of PF asymmetry. Most notably, the geomagnetic field asymmetry should lead to a roughly 30% larger conductance for the NH ionosphere, based on amplitude alone.

2. Results From Empirical Model

Using the empirical models for the NH and SH, plots of the hemispherically integrated PF are presented in the top panel of Figure 1, as a function of the IMF clock angle, for three different Dip angles. Examining the solid lines in the panel, it is apparent that the NH supports significantly more PF during southward IMF and local summer (Dip angle of 27° for the NH, and −27° for the SH). In this case the maximum (over clock angle) from the NH model is 30% more than the maximum from the SH model. However, during equinox (dashed lines, Dip angle of 0°) and local winter (dotted lines, Dip angle of −27° for the NH, and 27° for the SH) this percentage is decreased to 23% and 15%, respectively. The maximum in all cases is very near 180°, except for small offsets possibly associated with the GSM *y*-component of the IMF, which affects the two hemispheres in opposite ways, in accordance with the geometrical mirror symmetry. When the clock angle is near 0° the PF asymmetry appears absent, except in the case of local winter, when the PF levels are much lower.

Estimation of the parameters that define the models is subject to uncertainty associated with the finite size of the FAST data set. To bound the associated uncertainty in the integrated PF we divide the orbit-sets for each hemisphere into two non-intersecting sets, each half the size of the original set, by taking every other orbit from the time sequence of orbits. Hence, for each hemisphere we have the set of even orbits and the set of odd orbits, which have an essentially identical sampling of the epoch, but are non-intersecting. The modeling methodology is applied to these half-sized data sets to produce two new models for each hemisphere: the "even models" and the "odd models," which do not share any data.

The results from the even and odd models are presented in the left hand column of Figure 1. Roughly, we can interpret the region between the even and odd model estimates as the confidence interval for the original model estimate (top panel of Figure 1). In the vicinity of southward IMF, for local summer and equinox, the confidence intervals do not come close to overlapping, while for local winter they overlap just slightly. Also, the confidence intervals do not overlap in the vicinity of northward IMF during local winter, although the PF levels are much lower. A detailed analysis is given in Section 4.

A potential pitfall in making a conclusion based on these results is the possible existence of a systematic bias. The most likely source of systematic bias is FAST's precessing elliptical orbit, which may provide different NH and SH samplings of un-modeled parameters. A possibility suggested by one of the referees is a bias in the sampling of universal time (e.g., Billett et al. (2018)), and we have put a response in the Supporting Information S1. Here we consider the sampling of altitude. Although altitude is a modeled parameter, the NH and SH have very different altitude samplings, and so the model may not effectively compensate for the difference.

Histograms of the orbit altitudes for the NH and SH data sets are shown in the top two panels of Figure 2. It is evident that the SH orbits are, on average, much higher in altitude. Although the altitude parameter in the models should, in theory, compensate for the difference, it is possible that the sampling is so different that the compensation is not effective. (Note, we have evaluated both the NH and SH models at an altitude of 2,936 km, which is halfway between their median orbit altitudes.) To address this question the right-hand column of Figure 1 shows the altitude dependence of the integrated PF predicted by the models. It is seen that in all the cases where asymmetry is predicted, the integrated PF is predicted to increase with altitude, and this shows the tendency in the data. This prediction is consistent with the idea that downward PF can be converted to other forms of energy, such as particle kinetic energy flux, in the auroral acceleration region (e.g., Richmond (2010)). Therefore, if there is any bias it should be toward higher PF in the SH, which is opposite to the main observed effect, that is, the effect during southward IMF. However, the potential bias does place doubt on the evidence for the reversal of the effect during local winter and northward IMF, and so we do not make that conclusion.

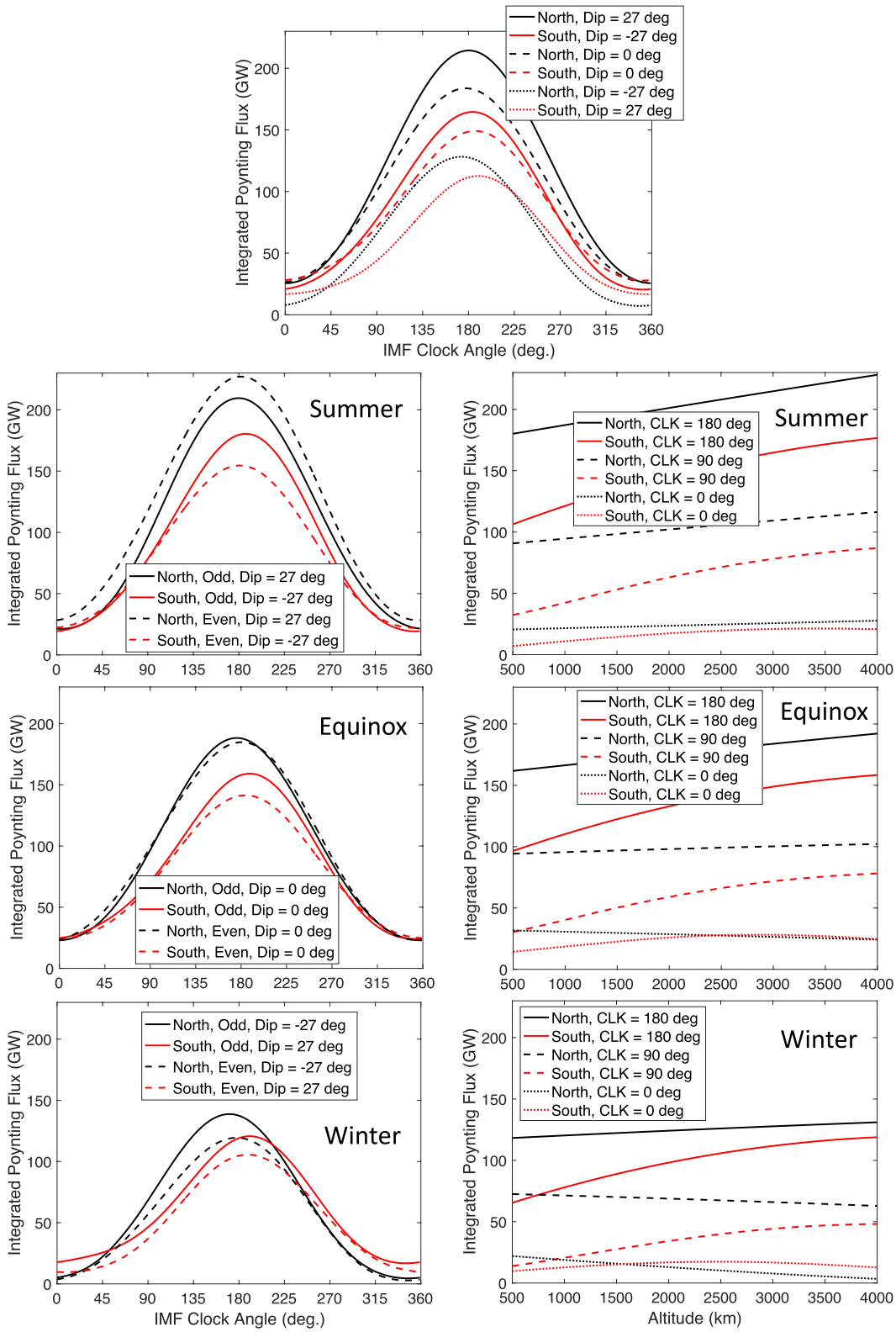

Figure 1. Model output for integrated Poynting flux, with the northern hemisphere in black and the southern hemisphere in red. The upper and left-hand panels show results as a function of interplanetary magnetic field clock angle, where the upper panel is for the full model, and the three left-hand panels are for the models constructed using the even and odd orbits. The three right-hand panels show results as a function of measurement altitude, where all fluxes have been projected to 100 km in altitude. From top to bottom, the rows show results for local summer, equinox, and local winter, whereas the top panel shows all three seasons together.

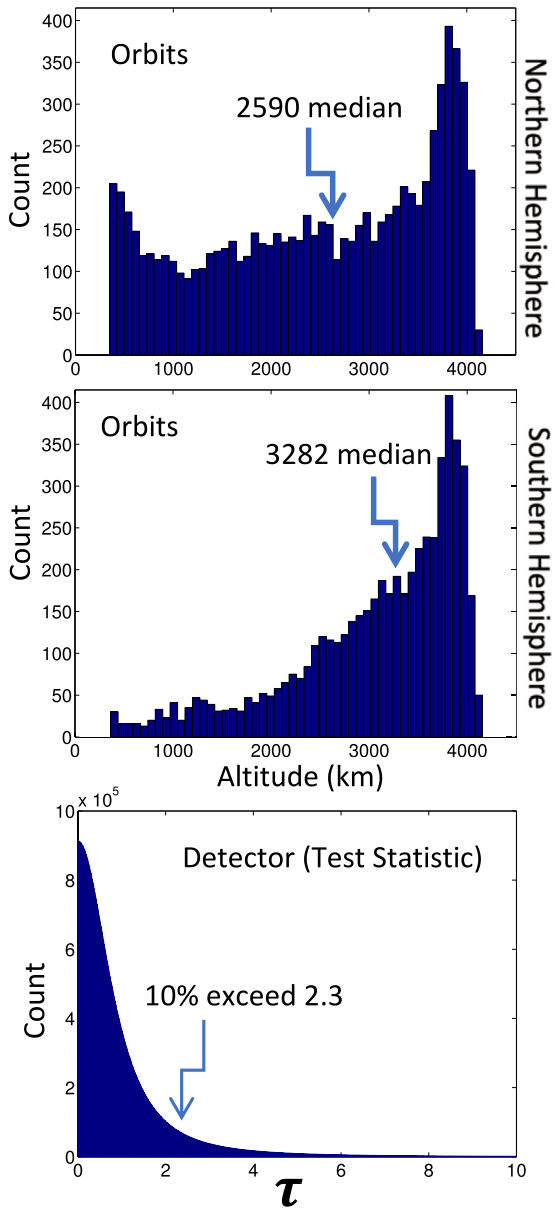

Figure 2. Histograms used in the study: The top two panels show altitude histograms for the orbits used in model making, for the northern (top panel) and southern (middle panel) hemispheres. The bottom panel shows the histogram for the test-statistic described in Section 4.

3. Results From Orbit Averaging

As a sanity check, the bottom four panels of Figure 3 show simple orbit-averages of the PF data for the NH and SH, without regard for the geophysical conditions. The data are averaged inside the cells of two 24 × 30 polar grids, one for the NH and one for the SH (bottom two panels), and then a smoothing algorithm is applied (middle two panels) for comparison with the model background states (top two panels of Figure 3).

The numbers in the top left corners of the panels of Figure 3 indicate the hemispherically integrated PF, which is 20% larger for the NH. Because the data is not sorted by the geophysical conditions, this slightly smaller asymmetry is consistent with the finding that the amount of asymmetry depends on the geophysical conditions, and that asymmetry is most severe under the most active conditions (southward IMF and local summer).

Figure 3 also suggests that the asymmetry arises from an asymmetry in the auroral-electrojet contribution, whereas the cusp contribution is actually greater for the SH. It appears that the NH tends to have a more fully developed two-cell convection pattern, and somewhat less energy flowing in through the cusp. The findings of Knipp et al. (2021) tend to support these findings, although lacking full coverage of the SH cusp region.

4. Analysis of Statistical Significance

Assuming there is no difference between the NH and SH (with respect to integrated PF under the Dip-angle and B_y mirror symmetries), the four PF peaks in the top-left panel of Figure 1, together with the two associated peaks in the upper panel, constitute six (non-independent) estimates for the PF peak during local summer. Similarly there are six estimates for equinox and six estimates for local winter. Each of these model estimates can be regarded as a random number drawn from a probability distribution function (PDF), with sample standard deviation determined according to the square-root of the number of data points used to form the model (ignoring the -1 in $\sqrt{N-1}$), and with mean equal to the actual value for the PF peak. From each of the three sets of six can be formed three statistically independent increments: (a) the difference between the peaks of the even and odd models for the NH (17.7 GW, 3.2 GW, 19.0 GW); (b) the difference between the peaks of the even and odd models for the SH (25.4 GW, 17.7 GW, 15.4 GW); and (c) the difference between the peaks of the full models for the northern and southern hemispheres (50.0 GW, 34.7 GW, 16.5 GW), where the numbers in parentheses are for local summer, equinox, and local winter, respectively. The statistical independence of the three increments is demonstrated in the Supporting Information S1.

Assuming Gaussian statistics, we will use a random number generator to simulate a large collection of increments and estimate the probability that the observed values could have occurred if the NH and SH are in fact the same. We have some options for comparing the increments. One approach is to form them into a single number (a test statistic) that increases according to the difference between the NH and SH, and then find the probability that the test statistic could be as large as observed under the assumption that there is no difference. This is a standard approach from statistical detection theory (e.g., Kay (1993)), and the test statistic is sometimes referred to as a detector.

Hence, consider the detector $\tau = |\Delta_3|/([|\Delta_1| + |\Delta_2|]/2)$, where Δ_j is the jth increment according to the numbering above. The NH to SH increment Δ_3 will be larger, on average, the more different are the NH and SH, whereas Δ_1 and Δ_2 are independent of the difference. Therefore, τ can be used as a detector for NH/SH asymmetry. By placing

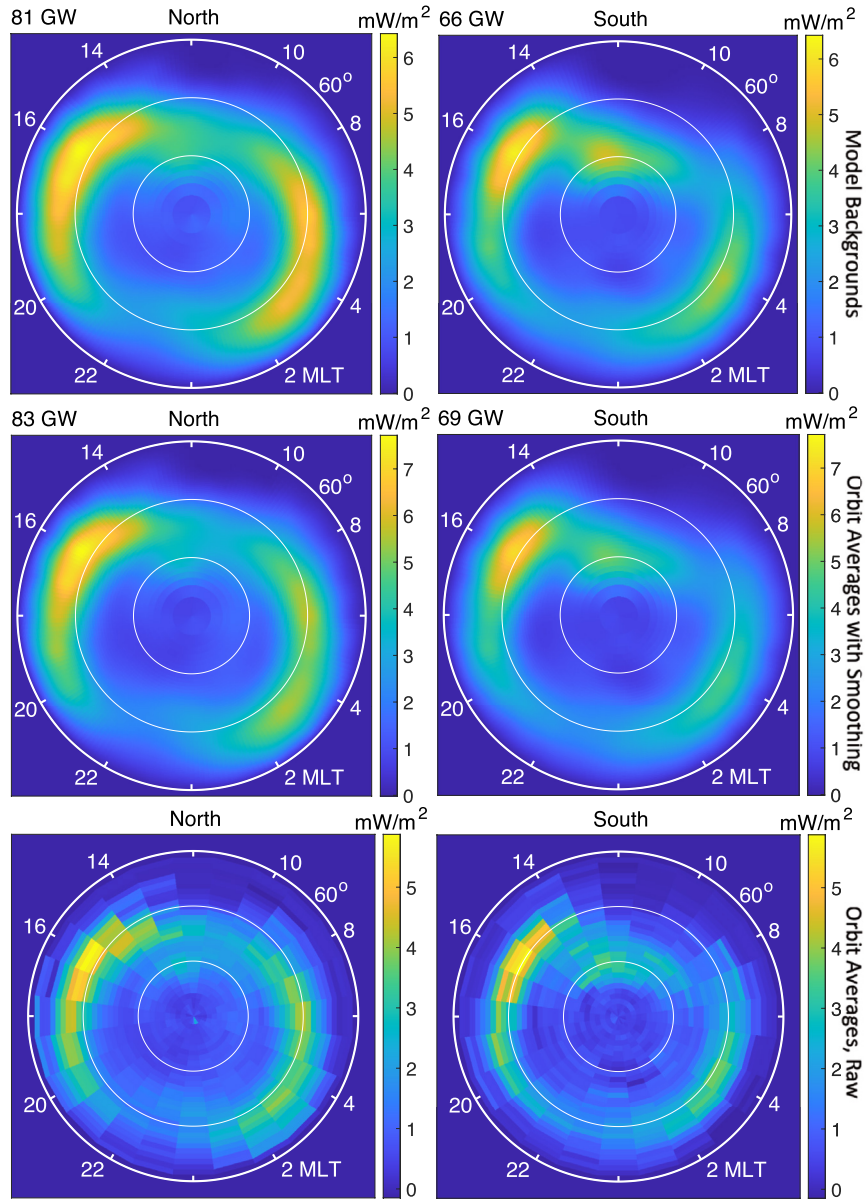

Figure 3. PF maps for the northern (left) and southern (right) hemispheres. The rows show the model backgrounds (top); the smoothed orbit averages for comparison to the backgrounds (middle); and the raw orbit averages (bottom).

Δ_1 and Δ_2 in the denominator of τ, its PDF can be calculated without knowing the absolute standard deviations for the Δ_j; it is only necessary to know the relative standard deviations, which can be estimated from the relative number of orbits used to make the various models.

Hence, to make a statistical analysis of τwe form six PDFs: (a) for the full NH model, (b) for the full SH model, (c) for the odd NH model, (d) for the even NH model, (e) for the odd SH model, and (f) for the even SH model. The first has standard deviation of $C/\sqrt{7301}$, the second has standard deviation of $C/\sqrt{4953}$, the third and fourth have standard deviations of $C/\sqrt{7301/2}$, and the fourth and fifth have standard deviations of $C/\sqrt{4953/2}$, where we have used the numbers of orbits from Section 1, and the constants C will cancel out upon forming τ. Assuming Gaussian statistics and using the Matlab random number generator, 100,000,000 samples are produced for each PDF, and then subtracted from each other to form the increments that go into τ. The resulting histogram for τ is shown in the third panel of Figure 2.

The value of τ calculated from the models (Figure 1) for local summer is $\tau = 50.0/([17.7 + 25.4]/2) = 2.3$. As indicated in the third panel of Figure 2, only 10% of the randomly generated test statistics are equal to or greater than 2.3. Therefore, if we were to conclude north-south asymmetry based on the "detection" criteria $\tau \geq 2.3$, there would be a 10% chance of making a false conclusion, for the case of local summer. Repeating the calculation for equinox and local winter, we find corresponding probabilities of 5% and 35%, respectively. Some additional commentary related to the 5% finding is given in the Supporting Information S1, and we have elected to present the 10% finding out of general conservatism.

5. Discussion and Conclusions

Comparing empirical models of PF for the NH and SH gives evidence that for southward IMF during local summer, there is significantly more downward PF in the NH, specifically, 30% more (Figure 1, top panel). The asymmetry arises primarily as an asymmetry in the auroral electrojet contribution, whereas the cusp contribution may actually be greater for the SH. This can be seen either in the model-generated PF patterns or in the orbit-averaged patterns shown in Figure 3, and similar findings have been presented by other authors (e.g., Shi et al. (2020)). The result suggests a difference in the nature or strength of the two cell convection pattern, for the NH and SH. During equinox and local winter the asymmetry percentages decrease to 23% and 15%, respectively.

Putting the question "Is there more downward PF in the NH?" into the framework of statistical detection theory, and assuming that Gaussian statistics apply to the model estimates, it is found that there is a 10% chance of making a false conclusion in the affirmative, for the case of local summer. The corresponding probability for equinox is even smaller (Section 4), although the asymmetry is not as great. However, the probability increases to 35% for local winter, and so we do not extend our conclusion of asymmetry to local winter.

The PDF for PF "events" is far from Gaussian (Cosgrove et al. (2014)). However, because model-fitting is essentially a process of averaging over many events, the central limit theorem should apply to the quantities assumed Gaussian in Section 4. The degree of convergence to Gaussian statistics remains as an unknown, and this is a weakness in the analysis of Section 4. Another weakness concerns the degree to which the PF is correlated from orbit to orbit, which affects the degree to which the even and odd orbit-sets are uncorrelated. However, the 7,301 orbits (and the 4,953 orbits) were selected from an original set of 20,000, which significantly reduces the number of back to back orbits. Neither weakness appears critical and so the computed false-alarm probability carries weight.

Although causes for asymmetry are not a major focus of this work, it seems appropriate to relate some basic observations. Since the result has been derived using a data set collected over 4.5 years, a first step in analysis is to divide the system into components that possess memory over this time scale, which can be considered as the conditions that might cause the asymmetry. Any components that do not persist over most of the 4.5 years cannot be considered as possible causes. For example, the configuration of Earth's geomagnetic field, and surface terrain with associated climate, are persistent conditions that seem the most likely cause of any hemispheric asymmetry. By contrast, if these conditions were to change abruptly, the magnetosphere and ionosphere would reconfigure within a time scale much less than 4.5 years, and probably less than an hour; there is no need to consider any long term memory in their configurations that could bias a data set collected over 4.5 years. Between these two extremes lies the sun and the solar wind it produces; it is less clear if these components possess any significant memory. However, since the model adjusts for the solar wind, it seems unlikely that the asymmetry results could be caused by any condition of the sun that favors Earth's NH over its SH.

From these basic considerations, let us focus now on Earth as the cause of asymmetry. The Dip angle is defined in the NH, and because the geomagnetic field is not actually a dipole field, this means that the effective (negated) Dip angle in the SH is actually somewhat different. The difference is on the order of the angle between the magnetic dipole and the axis of rotation. However, this variation is small compared to the variation from winter to summer, and so this should only slightly degrade the modeling of the SH Dip angle dependence. Given that the simple orbit averages (Figure 3) also show the asymmetry, and are not subject to this effect, we deem it to be minor.

Another consideration is that there is more wobbling of the Dip angle in the SH, due to a greater angle between the magnetic dipole and the axis of rotation. However, the period of this wobbling is 24 hr, whereas the time scale

for magnetosphere/ionosphere reconfiguration is thought much shorter, from as short as 10–20 min (Snekvik et al. (2017)), up to a couple of hours on the nightside (Anderson et al. (2014); Coxon et al. (2019)), with the longest times being associated with northward IMF (Fear and Milan (2012)). All of these reconfiguration timescales are much shorter than the time scale for the wobbling, and so it does not seem that the wobbling should disrupt the ionospheric state. Hence, one would think that the wobbling effect would average out with respect to integrated PF, assuming the response is relatively linear with changes in Dip angle. (A possible UTC bias in the FAST data set is discussed in the Supporting Information S1)

However, it is possible that the response is actually very non-linear, such that the wobbling effect does not average to zero. Pakhotin et al. (2021) have made an argument along these lines, and indicated the wobbling effect as a probable cause of the asymmetry they find. They argue that the wobbling affects the average ionospheric conductance, and thus leads to a different effect of MI-coupling in the two hemispheres. Greater conductance in the NH is also cited as a likely cause of the greater NH PF found by Knipp et al. (2021).

However, Knipp et al. (2021) also mention the possible importance of the fact that the field-aligned current configurations appear to be different in the two hemispheres, citing studies by Coxon et al. (2016), Shi et al. (2020), and Sangha et al. (2020). These findings are consistent with our finding that the two-cell convection pattern is more distinct in the NH, as can be seen in Figure 3, and a similar finding has been made by Förster and Haaland (2015). Given that we have argued for focusing on Earth as the source of the asymmetry, this leads us to ask what property of Earth might have a different and less regular distribution over the SH than over the NH. And this leads us back to the geomagnetic field, except with a focus on its distribution over the hemispheres, instead of on the wobbling effect. These distribution effects have been analyzed by Gasda and Richmond (1998), who find some potentially important differences between the two hemispheres. Förster and Haaland (2015) have invoked differing geomagnetic field distributions to explain the hemispherical asymmetry they find, and provide IGRF-derived maps of the geomagnetic field in their Figure 12.

Looking at Figure 12 from Förster and Haaland (2015) there are two apparent features: (a) The NH map is significantly more homogeneous over the polar cap and auroral region; and (b) the magnitude of the geomagnetic field is around 20% smaller in the NH, over most of this region. Feature (a) seems a likely explanation for the different appearance of the two-cell patterns in the two hemispheres, and one would expect that differing patterns imply differing integrated effects. However, Feature (2) suggests a potentially more direct explanation for the asymmetry: a 20% decrease in the geomagnetic field magnitude implies, according to Richmond (1995), a 30% increase in the ionospheric conductance. We also note that the magnetic anomaly (deviation from a dipole field) is a near-field effect, which decrease with distance (Laundal et al. (2017)), and so should have much less of an affect on phenomena occurring at great distances, such as magnetic reconnection.

Laundal et al. (2017) have analyzed the effects of north-south asymmetries in the geomagnetic field and refer to two studies of the geomagnetic-field-dependence of conductance. The study just mentioned by Richmond (1995) finds a dependence of $B^{-1.6}$, and a later study by Cnossen et al. (2011) finds a dependence of $B^{-1.5}$. These dependences are stronger than the B^{-1} dependence that would be derived from a simple analysis of the usual formulas for ionospheric conductance (e.g., Kelley (2009), and evaluating at the Pedersen peak). The Richmond (1995) result, for example, provides that a 20% smaller geomagnetic field produces a 30% larger conductance. The Laundal et al. (2017) paper also provides a map of the geomagnetic field asymmetry (their Figure 2) that supports the 20% difference that was inferred above from Figure 12 of Förster and Haaland (2015). Hence, based on magnetic field strength alone, the spatially-averaged conductance of the NH should be roughly 30% larger than that for the SH.

Therefore, while acknowledging that there exist other possibilities, we find two sources that seem especially likely for the asymmetry reported here: (a) the greater homogeneity of the geomagnetic field in the NH, which may produce a more pure two-cell convection pattern; and (b) the smaller geomagnetic field magnitude in the NH, which can be traced directly to a (roughly) 30% larger ionospheric conductance, and thus to a different effect of MI coupling.

Data Availability Statement

The geophysical parameters (time shifted to the magnetopause in a way consistent with (Weimer (2005)) are obtained from the OMNIWeb data set, available at https://omniweb.gsfc.nasa.gov/. The FAST data is available at http://sprg.ssl.berkeley.edu/fast/scienceprod/welcome.html.

Acknowledgments
RBC was partially supported by the Air Force Office of Scientific Research (AFOSR) under AFOSR Award No: FA9550-17-1-0258, and by NSF grant AGS-0922230. DJK was partially supported by NASA Award 80NSS-C20K1784 and AFOSR Award No. FA9550-17-1-0258. HB was partially supported by NSF grant AGS-0922230. ES was partially supported by NASA LWS Grant 80NSSC19K0081. We thank various members of the FAST team for supporting our access to the data.

References

Anderson, B. J., Korth, H., Waters, C. L., Green, D. L., Merkin, V. G., Barnes, R. J., & Dyrud, L. P. (2014). Development of large-scale birkeland currents determined from the active magnetosphere and planetary electrodynamics response experiment. *Geophysical Research Letters*, *41*, 3017–3025. https://doi.org/10.1002/2014GL059941

Billett, D. D., Grocott, A., Wild, J. A., Walach, M. T., & Kosch, M. J. (2018). Diurnal variations in global joule heating morphology and magnitude due to neutral winds. *Journal of Geophysical Research: Space*, *123*, 2398–2411. https://doi.org/10.1002/2017JA025141

Carlson, C. W., Pfaff, R. E., & Watzin, J. G. (1998). The fast auroral snapshot (fast) mission. *Geophysical Research Letters*, *25*(12), 2013–2016. https://doi.org/10.1029/98GL01592

Cnossen, I., & Förster, M. (2016). North-south asymmetries in the polar thermosphere-ionosphere system: Solar cycle and seasonal influences. *Journal of Geophysical Research: Space*, *121*(1), 612–627. https://doi.org/10.1002/2015ja021750

Cnossen, I., Richmond, A. D., Wiltberger, M., Wang, W., & Schmitt, P. (2011). The response of the coupled magnetosphere-ionosphere- thermosphere system to a 25. *Journal of Geophysical Research*, *116*, A12304. https://doi.org/10.1029/2011ja017063

Cosgrove, R. B. (2016). Does a localized plasma disturbance in the ionosphere evolve to electrostatic equilibrium? Evidence to the contrary. *Journal of Geophysical Research: Space*, *121*, 649–687. https://doi.org/10.1002/2015JA021672

Cosgrove, R. B., Bahcivan, H., Chen, S., Strangeway, R. J., Ortega, J., Alhassan, M., et al. (2014). Empirical model of Poynting flux derived from FAST data and a cusp signature. *Journal of Geophysical Research*, *119*, 411–430. https://doi.org/10.1002/2013JA019105

Coxon, J. C., Milan, S. E., Carter, J. A., Clausen, L. B. N., Korth, B. J. A. H., & Korth, H. (2016). Seasonal and diurnal variations in ampere observations of the birkeland currents compared to modeled results. *Journal of Geophysical Research: Space*, *121*, 4027–4040. https://doi.org/10.1002/2015JA022050

Coxon, J. C., Shore, R. M., Freeman, M. P., Fear, R. C., Browett, S. D., Smith, A. W., et al. (2019). Timescales of birkeland currents driven by the IMF. *Geophysical Research Letters*, *46*, 7893–7901. https://doi.org/10.1029/2018gl081658

Elphic, R. C., Means, J. D., Snare, R. C., Strangeway, R. J., Kepko, L., & Ergun, R. E. (2001). Magnetic field instruments for the fast auroral snapshot explorer. *Space Science Reviews*, *98*, 151–168. https://doi.org/10.1007/978-94-010-0332-2_6

Ergun, R. E., Carlson, C. W., Mozer, F. S., Delory, G. T., Temerin, M., McFadden, J. P., et al. (2001). The FAST satellite fields instrument. *Space Science Reviews*, *98*, 67–91. https://doi.org/10.1007/978-94-010-0332-2_3

Fear, R. C., & Milan, S. E. (2012). The IMF dependence of the local time of transpolar arcs: Implications for formation mechanism. *Journal of Geophysical Research*, *117*, AG03213. https://doi.org/10.1029/2011ja017209

Förster, M., & Haaland, S. (2015). Interhemispheric differences in ionospheric convection: Cluster EDI observations revisited. *Journal of Geophysical Research: Space*, *120*, 5805–5823. https://doi.org/10.1002/2014JA020774

Förster, M., Paschmann, G., Haaland, S. E., Quinn, J. M., Torbert, R. B., Vaith, H., & Kletzing, C. A. (2007). High-latitude plasma convection from Cluster EDI: Variances and solar wind correlations. *Annales Geophysicae*, *25*(7), 1691–1707. https://doi.org/10.5194/angeo-25-1691-2007

Gasda, S., & Richmond, A. D. (1998). Longitudinal and interhemispheric variations of auroral ionospheric electrodynamics in a realistic geomagnetic field. *Journal of Geophysical Research*, *103*(A3), 4011–4021. https://doi.org/10.1029/97ja03243

Hartinger, M. D., Moldwin, M. B., Zou, S., Bonnell, J. W., & Angelopoulos, V. (2015). Ulf wave electromagnetic energy flux into the ionosphere: Joule heating implications. *Journal of Geophysical Research: Space*, *120*, 494–510. https://doi.org/10.1002/2014JA020129

Hatch, S. M., LaBelle, J., Lotko, W., Chaston, C. C., & Zhang, B. (2017). Imf control of alfvénic energy transport and deposition at high latitudes. *Journal of Geophysical Research: Space*, *122*, 12189–12211. https://doi.org/10.1002/2017JA024175

Hong, Y., Deng, Y., Zhu, Q., Maute, A., Sheng, C., Welling, D., & Lopez, R. (2021). Impacts of different causes on the inter-hemispheric asymmetry of ionosphere-thermosphere system at mid- and high-latitudes: Gitm simulations. *Space Weather*, *19*, e2021SW002856. https://doi.org/10.1029/2021sw002856

Janhunen, P., Olsson, A., Tsyganenko, N. A., Russell, C. T., Laakso, H., & Blomberg, L. (2005). Statistics of a parallel poynting vector in the auroral zone as a function of altitude using polar efi and mfe data and astrid-2 emma data. *Annales Geophysicae*, *23*, 1797–1806. https://doi.org/10.5194/angeo-23-1797-2005

Kay, S. (1993). *Fundamentals of statistical signal processing: Detection theory*. Prentice Hall PTR.

Keiling, A. (2021). The dynamics of the alfvénic oval. *Journal of Atmospheric and Solar-Terrestrial Physics*, *219*, 105616. https://doi.org/10.1016/j.jastp.2021.105616

Keiling, A., Thaller, S., Wygant, J., & Dombeck, J. (2019). Assessing the global alfven wave power flow into and out of the auroral acceleration region during geomagnetic storms. *Science Advances*, *5*(6). https://doi.org/10.1126/sciadv.aav8411

Kelley, M. C. (2009). *Earth's ionosphere, plasma physics and electrodynamics* (2nd ed.). Academic Press.

Knipp, D., Kilcommons, L., Hairston, M., & Coley, W. R. (2021). Hemispheric asymmetries in poynting flux derived from dmsp spacecraft. *Geophysical Research Letters*, *48*. https://doi.org/10.1029/2021GL094781

Laundal, K. M., Cnossen, I., Milan, S. E., Haaland, S. E., Coxon, J., Pedatella, N. M., et al. (2017). North–south asymmetries in Earth's magnetic field effects on high-latitude geospace. *Space Science Reviews*, *206*, 225–257. https://doi.org/10.1007/s11214-016-0273-0

Liou, K., & Mitchell, E. J. (2020). Hemispheric asymmetry of the dayside aurora due to imbalanced solar insolation. *Scientific Reports*, *10*(1), 451. https://doi.org/10.1038/s41598-020-70018-w

Luhr, H., Park, J., Gjerloev, J. W., Rauberg, J., Michaelis, I., Merayo, J. M. G., & Brauer, P. (2015). Field-aligned currents' scale analysis performed with the swarm constellation. *Geophysical Research Letters*, *42*, 1–8. https://doi.org/10.1002/2014GL062453

Lysak, R., & Dum, C. (1983). Dynamics of magnetosphere-ionosphere coupling including turbulent transport. *Journal of Geophysical Research*, *107*, 1352. https://doi.org/10.1029/ja088ia01p00365

Pakhotin, I. P., Knudsen, D. J., Lysak, R. L., Burchill, J. K., & Burchill, J. K. (2020). Diagnosing the role of Alfvén waves in global field-aligned current system dynamics during southward imf: Swarm observations. *Journal of Geophysical Research: Space*, *125*, e2019JA027277. https://doi.org/10.1029/2019JA027277

Pakhotin, I. P., Mann, I. R., Lysak, R. L., Knudsen, D. J., Gjerloev, J. W., Rae, I. J., et al. (2018). Diagnosing the role of Alfvén waves in magnetosphere- ionosphere coupling: Swarm observations of large amplitude nonstationary magnetic perturbations during an interval of northward imf. *J. Geophys. Res., Space*, *123*, 326–340. https://doi.org/10.1002/2017JA024713

Pakhotin, I. P., Mann, I. R., Xie, K., & Knudsen, D. J. (2021). Northern preference for terrestrial electromagnetic energy input from space weather. *Nature Communications*, *12*. https://doi.org/10.1038/s41467-020-20450-3

Papitashvili, V. O., & Rich, F. J. (2002). High-latitude ionospheric convection models derived from defense meteorological satellite program ion drift observations and parameterized by the interplanetary magnetic field strength and direction. *Journal of Geophysical Research*, *107*(A8), 1198. https://doi.org/10.1029/2001ja000264

Pettigrew, E. D., Shepherd, S. G., & Ruohoniemi, J. M. (2010). Climatological patterns of high-latitude convection in the northern and southern hemispheres: Dipole tilt dependencies and interhemispheric comparisons. *Journal of Geophysical Research*, *115*, 956. https://doi.org/10.1029/2009ja014956

Richmond, A. D. (1995). In H. Volland (Ed.), *Ionospheric electrodynamics* (pp. 249–290). CRC Press (ISBN: 9780849325205).

Richmond, A. D. (2010). On the ionospheric application of Poynting's theorem. *Journal of Geophysical Research*, *115*, A10311. https://doi.org/10.1029/2010JA015768

Sangha, H., Milan, S. E., Carter, J. A., Fogg, A. R., Anderson, B. J., Korth, H., & Paxton, L. J. (2020). Bifurcated region 2 field-aligned currents associated with substorms. *Journal Geophysical Research: Space*, *125*, e2019JA027041. https://doi.org/10.1029/2019JA027041

Shi, Y., Knipp, D. J., Matsuo, T., Kilcommons, L., & Anderson, B. (2020). Modes of (facs) variability and their hemispheric asymmetry revealed by inverse and assimilative analysis of iridium magnetometer data. *Journal Geophysical Research: Space*, *125*, e2019JA027265. https://doi.org/10.1029/2019JA027265

Snekvik, K., Østgaard, N., Tenfjord, P., Reistad, J. P., Laundal, K. M., Milan, S. E., & Haaland, S. E. (2017). Dayside and nightside magnetic field responses at 780 km altitude to dayside reconnection. *Journal of Geophysical Research: Space*, *122*, 1670–1689. https://doi.org/10.1002/2016JA023177

Stubbs, T. J., Vondrak, R. R., Østgaard, N., Sigwarth, J. B., & Frank, L. A. (2005). Simultaneous observations of the auroral ovals in both hemispheres under varying conditions. *Geophysical Research Letters*, *32*, L03103. https://doi.org/10.1029/2004gl021199

Weimer, D. (2005). Improved ionospheric electrodynamic models and application to calculating joule heating rates. *Journal of Geophysical Research*, *110*, A05306. https://doi.org/10.1029/2004JA010884

Wing, S., Ohtani, S., Newell, P. T., Higuchi, T., Ueno, G., & Weygand, J. M. (2010). Dayside field- aligned current source regions. *Journal of Geophysical Research*, *115*, A12215. https://doi.org/10.1029/2010ja015837

Workayehu, A. B., Vanhamäki, H., & Aikio, A. T. (2019). Field-aligned and horizontal currents in the northern and southern hemispheres from the swarm satellite. *Journal of Geophysical Research: Space*, *124*, 7231–7246. https://doi.org/10.1029/2019JA026835